Journal of Information and Data Management, 2025, 16:1, doi: 10.5753/jidm.2025.4181

Detailed Mapping of Irrigated Rice Fields Using Remote Sensing data and Segmentation Techniques: A case of study in Turvo, Santa Catarina, Brazil

Andre Dalla Bernardina Garcia [**Programa de Pós-Graduação em Sensoriamento Remoto (PGSER), Coordenação de Ensino, Pesquisa e Extensão (COEPE), Instituto Nacional de Pesquisas Espaciais (INPE)** | ***andre.garcia@inpe.br***]
Victor Hugo Rohden Prudente [**University of Michigan (UofM), School for Environment and Sustainability** | ***victorrp@umich.edu***]
Darlan Teles da Silva [**Programa de Pós-Graduação em Sensoriamento Remoto (PGSER), Coordenação de Ensino, Pesquisa e Extensão (COEPE), Instituto Nacional de Pesquisas Espaciais (INPE)** | ***darlan.silva@inpe.br***]
Michel Eustáquio Dantas Chaves [**São Paulo State University (UNESP), School of Sciences and Engineering, Tupã** | ***michel.dantas@unesp.br***]
Kleber Trabaquini [**Santa Catarina Agricultural Research and Extension Corporation (EPAGRI)** | ***klebertrabaquini@epagri.sc.gov.br***]
Ieda Del'Arco Sanches [**Programa de Pós-Graduação em Sensoriamento Remoto (PGSER), Coordenação de Ensino, Pesquisa e Extensão (COEPE), Instituto Nacional de Pesquisas Espaciais (INPE); Divisão de Observação da Terra e Geoinformática (DIOTG), Coordenação Geral de Ciências da Terra (CG-CT)** | ***ieda.sanches@inpe.br***]

Programa de Pós-Graduação em Sensoriamento Remoto (PGSER), Coordenação de Ensino, Pesquisa e Extensão (COEPE), Instituto Nacional de Pesquisas Espaciais (INPE), Av. dos Astronautas, 1758 - São José dos Campos - SP - Brazil

Received: 1 March 2024 • **Published:** 27 January 2025

Abstract
In this study, we evaluated multiple methods and data sources for mapping irrigated rice fields in Turvo, Santa Catarina, using a detailed reference map that includes irrigation channels, roads, and boundaries within and between rice fields. We tested different approaches using a per-pixel and segmentation approaches. In the per-pixel classifications scenarios we used a a Random Forest (RF) applied to the China-Brazil Earth-Resources Satellite Multispectral and Panchromatic Wide-Scan Camera (CBERS-4A/WPM) data, and to Sentinel-2 (S2) imagery. For the segmentation approach we used a combination of S2 imagery with a Segment Anything Model geospatial (Samgeo) mask applied to high-resolution CBERS-4A/WPM data (S2+WPM/Samgeo). We qualitatively and quantitatively compared maps derived from a existing source (MapBiomas) with our scenarios. MapBiomas and per-pixel S2 classification provided adequate general plot boundary identification, however, lacked finer details. CBERS-4A/WPM data captured some of these details, although they showed a high rate of false positives due to confusion with other vegetation types. We also examined how detailed rice field mapping affected time-series analysis. Our findings indicate that the S2+WPM/Samgeo approach most closely matched the reference map time-series and offered superior detail, better distinguishing field heterogeneities. This method could support more detailed and accurate monitoring of rice fields. Overall, S2+WPM/Samgeo delivered the most precise and detailed mapping of irrigated rice in the region.

Keywords: CBERS-4A/WPM, Sentinel-2, Time Series, Agriculture, Segment Anything Model

1 Introduction

Rice is one of the most relevant grains crops that humankind grows [Macarini *et al*., 2019] [Crisóstomo de Castro Filho *et al*., 2020] [Laborte *et al*., 2017], and it has been present in the food systems of many different countries worldwide, including Brazil. According to the United Nations Food and Agriculture Organization Statistical Databases [FAO, 2022], from 1994 to 2020, rice was the tenth most produced crop in the world, with 660 million tons produced. Brazil has an annual average production of 11.2 million tons of rice and is the only non-Asian country on the list [de Bem *et al*., 2021]. Rio Grande do Sul (RS) and Santa Catarina (SC) are the prominent Brazilian rice producer states, with 8 million tons and 1.2 million tons, respectively [ANA, 2020]. In this context, obtaining accurate geolocation of rice fields is highly desirable to provide reliable information to mitigate the impacts of climate change and food insecurity [Crisóstomo de Castro Filho *et al*., 2020] [Lobell *et al*., 2008] [de Bem *et al*., 2021].

Remote Sensing (RS) technology has been used to obtain detailed information about crops in different studies [Amani *et al*., 2020] [Beriaux *et al*., 2021] [Boschetti *et al*., 2017] [Crisóstomo de Castro Filho *et al*., 2020] [Cucho-Padin *et al*., 2020] [de Bem *et al*., 2021] [Meng *et al*., 2021] [Zhang *et al*., 2018a] [Zhang *et al*., 2019]. With RS, it is possible to monitor large areas in a less cost-effective way than traditional survey approaches. However, generally, there is a trade-off between mapping large areas and providing detailed features. Monitoring each individual field is important for accurate estimates and for guiding farms to individual field management. The more traditional mapping using the common free satellite data has limitations on spatial (10 to 30 meters) and temporal resolution (5 to 16 days), which negatively impacts the accuracy of identifying single fields. Data from satellites such as Landsat/National Aeronautics and Space Administration (NASA) (30 meters, 16 days) or Sentinel-2/European Space Agency (ESA) (10-20 meters, 5 days) cannot map

field boundaries in a high level of detail. The mapping using these satellites generally incorporates small roads and irrigation water channels (< 10 meters) as part of the rice fields. This misincorporation can interfere with the classification metrics of rice fields and, therefore, with other official statistics.

An essential phase to define agricultural fields is the accurate identification of the field boundaries. Generally, two main categories are commonly employed for this task. The first one involves using edge detection techniques to detect discontinuities in pixels exhibiting significant variations in values. Examples of such algorithms involve more simple filters like Sobel [Wen *et al*., 2022] and Scharr [Watkins and Van Niekerk, 2019], as well as more complex filters like Canny operators [Zhang *et al*., 2018b; Xiao *et al*., 2021]. The second category consists of image segmentation techniques, ranging from traditional, unsupervised computer vision algorithms to advanced deep learning models. Conventional computer vision algorithms, such as Simple Linear Iterative Clustering (SLIC) [Clauss *et al*., 2018; Zhang *et al*., 2018b], Multi-Resolution Segmentation (MRS) [Li *et al*., 2015; Tang *et al*., 2020], and the Watershed segmentation algorithm [Xue *et al*., 2021] that produce a single connected and closed pixel region, are commonly used for agricultural crop type classification. Nevertheless, these segmenters frequently encounter challenges with parameter configuration, where determining the best parameters can be a susceptible-to-error process, potentially resulting in less than ideal outcomes.

In recent years, deep learning models and neural networks have gained traction for satellite image segmentation tasks [Masoud *et al*., 2019; Garcia-Pedrero *et al*., 2019; Waldner and Diakogiannis, 2020]. Despite this, these models typically necessitate extensive collections of images and task-specific training samples, which restricts their ability to generalize across various regions and types of land cover. In this context, the newly introduced Segment Anything Model (SAM) [Kirillov *et al*., 2023] stands out, since it already holds a comprehensive collection of training images and delivers a very good performance for zero-shot segmentation tasks.

The modified version of SAM for geo-information data (Samgeo) [Wu and Osco, 2023b] simplifies its use for remote sensing applications [Osco *et al*., 2023]. We adopted the general segmentation approach, whereby SAM segmented various objects without guided prompts. This method segments all potential objects within images, including those without ground-truth labels. As it lacks guidance, it may also produce segments for unknown classes, functioning as a conventional segmentation filter. Samgeo offers several pre-trained ViT, including ViT-H, ViT-L, and ViT-B. These models exhibit varying computational demands and possess different underlying architectures. We used the ViT-H SAM model, the most advanced and accessible in this package.

In this way, our study aims to identify and delineate irrigated rice fields in Turvo, Santa Catarina state in the southern part of Brazil. For that, we combined the use of the Samgeo segmentation tool in images from Multispectral and Panchromatic Wide-Scan Camera (WPM) sensor onboard the China-Brazil Earth Resources Satellite-4A (CBERS-4A) with data from Sentinel-2/MSI (MultiSpectral Instrument). We compared the gain of this approach with per-pixel classifications based on i) only Sentinel-2/MSI data, ii) only CBERS-4A/WPM data, and iii) with the map of the Mapbiomas initiative [MapBiomas, 2023]. The objective of this study was to evaluate the impact of a more detailed segmentation in rice irrigated fields along with the use of Samgeo to minimize inclusion errors in the final demarcation of irrigated rice plots. This paper is an extended version of [Garcia *et al*., 2023], presented at the XXIV Brazilian Symposium on GeoInformatics (GEOINFO 2023).

2 Material and Methods

2.1 Study Area

Our study area is the municipality of Turvo, located in the southern Santa Catarina region (SC), Brazil (see **Figure 1**). Turvo is the major rice producer within this relevant region for irrigated rice cultivation in SC. A substantial portion, 50.7%, of the entire region is dedicated to rice cultivation, corresponding to approximately 11.9 thousand hectares of land. Turvo has a humid subtropical climate characterized by hot summers and an average annual temperature ranging from 19°C to 20°C. The total annual precipitation average reaches approximately 1,800 mm. Throughout the year, relative air humidity remains consistently above 80%. The rainfall distribution is generally well balanced, although tends to be more concentrated between May and August [Wrege *et al*., 2012].

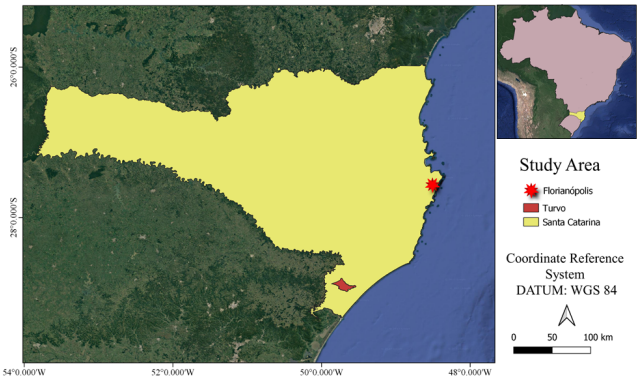

Figure 1. Location of the study area in the state of Santa Catarina, highlighting Florianópolis, the state capital, and Turvo, in the Southern region.

In Santa Catarina, irrigated rice cultivation is found in three principal regions, Northern, Itajaí Valley, and Southern. For our Region of Interest (ROI), the cultivation ranges from August to April. For Turvo, rice management and phenological stages can be divided into Sowing (S) and Emergence (E) which occur between August and November, Vegetative Development (VD) phase is observable between September and December, Flowering (F) usually occurs in the summer between December and January, Grain Filling (GF) occurs between January and February followed by Maturation (M) and Harvest (H) which can take place between late February and April [CONAB, 2023].

2.2 Satellite Data

We used data from two optical sensors to perform this study. The first sensor was the Multispectral and Panchromatic Wide-Scan Camera (WPM) onboard the China-Brazil Earth-Resources Satellite (CBERS-4A), freely available in the image catalog of the National Institute for Space Research (INPE). CBERS-4A/WPM has five spectral bands (see **Table 1**). Due to the low temporal resolution of CBERS-4A/WPM (31 days) and the high frequency of cloud cover in the region [Prudente *et al*., 2020], only a single cloud-free image from September 26, 2021, was utilized for segmentation. This date corresponds to the period of soil preparation and rice crop planting (see Section 2.1), the optimal time frame to identify agricultural fields. In Turvo, this period extends from early August to late November [CONAB, 2023].

Table 1. CBERS-4A/WPM spectral bands used in this study.

Spectral bands (µm)	Resolution (m/px)	Band ID
Blue (0.45-0.52)	8	1
Green (0.52-0.59)	8	2
Red (0.63-0.69)	8	3
NIR (0.77-0.89)	8	4
Panchromatic (0.45-0.90)	2	P

Note: NIR = Near Infrared.

The second sensor was the Multispectral Instrument (MSI) onboard the Sentinel-2A and 2B satellites, obtained through the ”COPERNICUS/S2_SR_HARMONIZED” collection on the Google Earth Engine (GEE) platform [Gorelick *et al*., 2017]. The Sentinel-2/MSI has 13 spectral bands. However, we used only six for this study (see **Table 2**).

Table 2. Sentinel-2/MSI spectral bands used in the study.

Spectral bands (µm)	Resolution (m/px)	Band ID
Blue (0.45-0.52)	10	B2
Green (0.54-0.57)	10	B3
Red (0.65-0.68)	10	B4
NIR (0.78-0.89)	10	B8
SWIR 1 (1.56–1.65)	20	B11
SWIR 2 (2.10–2.28)	20	B12

Note: NIR = Near Infrared, SWIR = Shortwave Infrared

2.3 Reference data creation

Based on the expert’s domain in the field, polygons representing irrigated rice fields and non-rice areas in the region were drawn manually. For this purpose, we used a 2x2 meters pansharpening image of CBERS4A/WPM from the beginning of the rice reproductive cycle (2021-09-26), together with a mosaic of high-resolution images obtained using Google Earth Pro software, dated December 2021, on the Quantum Geographic Information System (QGIS v.3.10) platform. Initially, the polygon boundaries were delineated using CBERS4A/WPM 2x2 meters images, however, in case of doubt, we refer to Google images to ensure the correct delineation of the boundaries, channels, roads and borders of the irrigated rice fields. Due to the level of detail required for the reference map, covering a manual vectorization for our entire study area would require a lot of time and labor effort. For this reason, we created a grid of 5x5 km and randomly chosen five representative blocks for the vectorization process. This area served as a guide to delineate the reference areas.

After delineating the rice and non-rice areas, the vector data were converted to raster data for evaluation and comparison with binary mappings produced by different classification methods. Since irrigation channels, roads, and borders of rice fields have a narrow width, between 2 and 3 meters, we defined the pixel size as 2x2 meters, with the Coordinate Reference System (CRS) set to EPSG: 32722, in order to maintain these characteristics in the raster field map.

2.4 Irrigated rice maps

In the following sections, we will discuss in detail how the binary maps of irrigated rice were obtained. In **Figure 2**, we illustrate the general step-by-step process to obtain these maps. We conducted a qualitative analysis of the land use and land cover map to verify which classes cause the most confusion between non-rice classes and also which ones most closely resemble irrigated rice. In addition, we obtained time series for each class within the initial development period of irrigated rice in the region.

2.4.1 Mapbiomas irrigated rice map

In order to compare our detailed mapping approach of irrigated rice fields and our reference map with different products and classification methods, we used the Mapbiomas mapping for the year 2021. The Mapbiomas product is based on Landsat image mosaics with a spatial resolution of 30x30 meters and aims to map the entire Brazilian territory. For a complete description of the mapping methodology, it is recommended to refer to the Handbook [MapBiomas, 2023]. The Collection 8 used contains more than 30 thematic classes, including the subclass of irrigated rice (”id” = 40). Therefore, for this work, thematic subclass 40 was reclassified as 1, and all other classes were reclassified to the value 2 (see **Figure 2**), thus producing a binary map of rice and non-rice with a resolution of pixel of 30 meters, which was resized using the Warp method in QGIS software v.3.10.

To ensure that the matrices/grids of all classified images have the same size and number of pixels, and that each pixel corresponds exactly to its reference pixel in the ground truth map, an algorithm was used to reproject the pixels of the binary maps with a pixel size of 2x2m into the Coordinate Reference System (CRS) set to EPSG:32722. This procedure did not aim to enhance or diminish the scale of the reference maps, instead, it aimed to establish alignment and consistency among the images.

2.4.2 CBERS-4A/WPM irrigated rice map

A mapping using an image generated by the WPM sensor of CBERS-4A was also employed, aiming to take advantage of the good spatial resolution of 8 meters per pixel of the blue, green, red, and near-infrared bands to assess whether it is

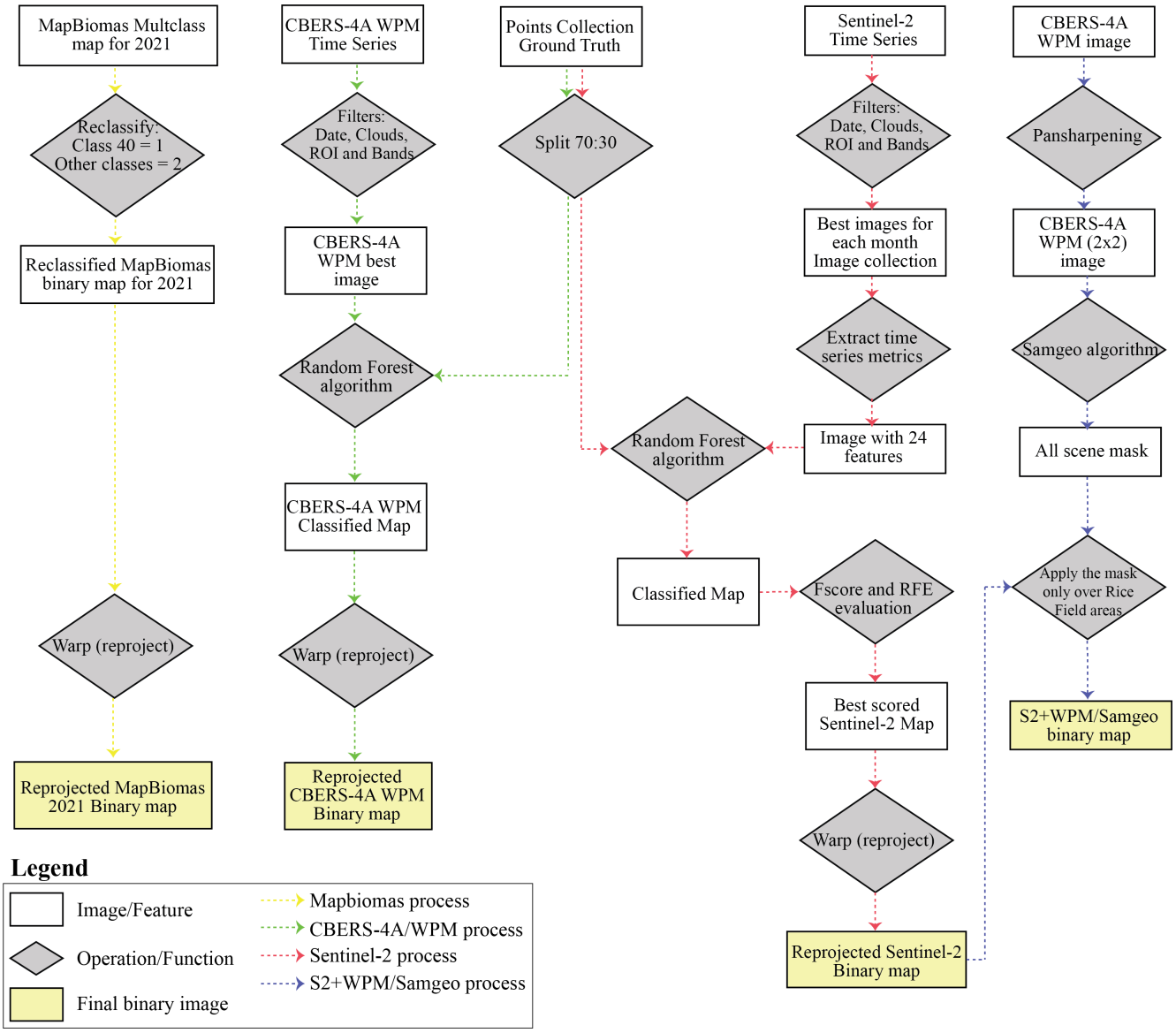

Figure 2. Flowchart of binary classifications of irrigated rice from different approaches.

possible to classify the irrigated rice fields in detail considering irrigation channels, boundaries, and roads, using only a single available image for the period.

To produce the binary map, the composite image of 4 bands was loaded into the Google Earth Engine (GEE) platform, and we utilized a Random Forest algorithm through the ”ee.Classifier.smileRandomForest()” function to classify the pixels into irrigated rice and non-irrigated rice. The native Random Forest function of GEE has only six parameters for model adjustment, including ”numberOfTrees,” ”variablesPerSplit,” ”minLeafPopulation,” ”bagFraction,” ”maxNodes,” and ”seed.” In both classifications that used this algorithm, we only modified the parameters ”numberOfTrees” and ”seed” to 1. For CBERS-4A/WPM, considering the [Oshiro *et al.*, 2012] study information and our previous exploratory analysis with 20, 50, and 100 trees, a value of 20 for ”numberOfTrees” was selected as the most suitable choice due to the small dataset we had for CBERS-4A/WPM classification. The previous study conducted by [Oshiro *et al.*, 2012] with 29 different datasets concluded that beyond 128 trees, there is no significant improvement in the model’s performance. The authors also highlight that for medium-sized datasets, the ideal range of trees is between 64 and 128, while for small datasets, 8 trees or more are sufficient.

Based on experts domain 4,000 points were selected within the area of interest and labels were added to them under the category ”LULC,” with a value of one (1) designated for pixels representing irrigated rice and two (2) for all other types of objects in the scene. Similarly to the process used for the MapBiomas map, here the raster matrix data was also resized using the Warp algorithm of QGIS software version 3.10, ensuring that the pixels corresponded to the reference map.

2.4.3 Sentinel-2 irrigated rice map

For mapping using Sentinel-2 images based on the Multi-Spectral Instrument (MSI) sensor, cloud-free images were filtered, considering only the period between July and December, during which rice is in the early development stage

(from soil preparation to peak vegetative growth). The selected images, one for each month, correspond to the following dates: July 18, 2021; August 22, 2021; September 26, 2021; October 26, 2021; November 25, 2021; and December 20, 2021.

Since the SWIR bands have a spatial resolution of 20 m, we used a resampling and reprojection algorithm within the GEE platform to match the other 10 m resolution bands used. For details on the resampling step functions, see the guide developed by GEE team [Google, 2024] and to our github link at the end of this paper.

The temporal series of images were reduced in GEE using the mean (.mean() function), standard deviation (.std_dev() function), maximum (.max() function) and minimum (.min() function). After applying the reducers to each band of the 6 images, we obtained 24 temporal features (4 metric for each band) that were combined and stacked into a single image for use in the Random Forest classifier.

The same set of points used for the mapping based on the CBERS-4A WPM image was also used here, after confirming that the points were correctly labeled. After this process, they were divided into 70% for training and 30% for validation and testing.

The Random Forest algorithm was implemented on the Google Earth Engine platform using the "ee.Classifier.smileRandomForest()" function, the same step described in Section 2.4.2) to CBERS-4A/WPM data. Taking into account the information highlighted by [Oshiro *et al*., 2012] and the analyzes performed (ntree = 20, ntree = 50, and ntree = 100), a value of 50 trees was selected as the most suitable choice.

The other parameters of the function were set as default, except for the "seed" parameter, which was defined as the value 1, similar to what was done for the classification of the image obtained from the CBERS-4A/WPM. Following the process used for other binary map classifications, the raster matrix data was resized using the Warp algorithm of QGIS software version 3.10, ensuring that the pixels corresponded to the reference map.

The importance of each variable was calculated by the sum of the decrease in the Gini impurity index on all trees in the forest. Each time a node is split based on a variable, the impurity criterion for the descendant nodes is consistently lower than that of the parent node [Jiang *et al*., 2019]. The sum of these decreases for each variable across all trees in the forest provides a rapid and reliable assessment of variable importance. After computing all importance, the Feature Score (FSCORE) and Recursive Feature Elimination (RFE) methodologies are applied to find the most accurate classification map based on the number of variables [Bazzan *et al*., 2022; Badda *et al*., 2023].

To identify which thematic classes cause the most confusion with irrigated rice, which is the subject of the study, we generate a parallel LULC classification, we used the Sentinel-2 image collection to create a land use and land cover map with 7 classes: irrigated rice, forest, fallow land, other crops, built-up areas, pasture, and water. The purpose of this map was to identify which thematic classes cause the most confusion with irrigated rice, which is the subject of the study. We used 378 points, distributed as follows: 100 points for rice, 52 points for other crops, 36 for built-up areas, 50 for water, 50 for forest, 48 for pasture and 42 for fallow land. We reduced the number of irrigated rice points to avoid class imbalance in the model.

2.4.4 S2+WPM/Samgeo irrigated rice map

Within the rice cultivation period, from August 1st to May 30th, only the tiles identified as WPM205149 and WPM205150 cover the region of interest, delimited by the boundary box [610301.5645096592, 643079.4595588772, 6792884.760658602, 6813189.905747686 [EPSG: 32722]]. A total of 10 images were found for the region of interest, at the L4 processing level, meaning images already orthorectified with radiometric and geometric correction of the system refined by the use of control points and a digital terrain model. However, only the image "CBERS4A_WPM20514920210926" fully covers the study area and does not have clouds. The image "CBERS4A_WPM20515020210926", although suitable regarding clouds, covers only the lower/southern third of the region of interest. Once the image to be used was defined, the Blue, Green, Red, NIR, and Pan bands belonging to this tile and date were downloaded. A three-band composition was created using the red, green and blue bands, with a resolution of 8x8 meters, as illustrated in **Figure 3**. This same composition was used to generate a 2x2 meters image using a pansharpening approach, using an algorithm from the Geospatial Data Abstraction Library (GDAL) library [GDAL and OGR, 2024] within QGIS, as illustrated in **Figure 3**. Currently, the only pansharpening algorithm supported in the GDAL package used is a "weighted" Brovey algorithm, and among the available resampling methods, a cubic convolution method was applied, based on the results obtained by [Li *et al*., 2017] for agricultural areas.

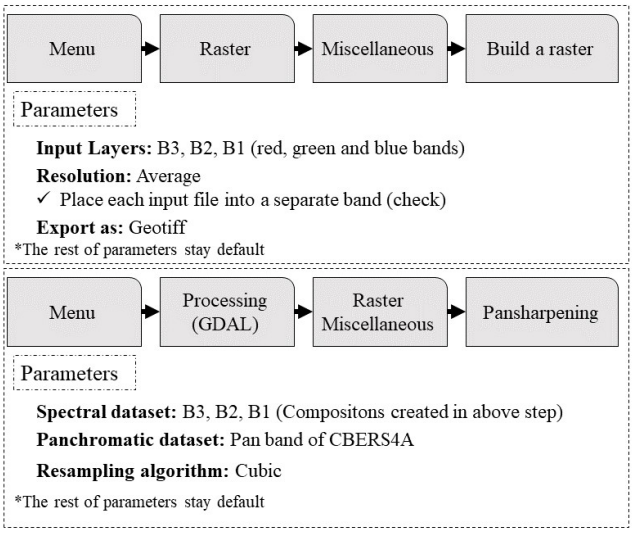

Figure 3. Menus and step by step guide to create a pansharpening composition in QGIS.

After the pansharpening process, the image was converted to the integer type (uint8) with values ranging from 0 to 255 for the pixels. This conversion is necessary since the Samgeo package uses dependencies such as pyTorch, where, typ-

ically, images of dtype torch. uint8 are expected to have values in the range of 0 to 255 [Wu and Osco, 2023a]. To perform this conversion, we used a Python script that can be accessed by following the link to the repository at the end of this article. With the prepared image, Google Drive was used to upload and store the image in the cloud, so that it could be processed using the Google Colab platform. In addition to the functions for importing and loading the packages used for visualization and image loading, we also used functions belonging to the Samgeo package to obtain the feature mask of our study area. For a detailed explanation of the code used, we recommend accessing the GitHub repository available at the end of the article.

As in this work, the intention was to use the Samgeo package in a zero-shot approach, and we also chose to leave the fine-tuning parameters according to the default established by the package developers. However, it is possible to adjust the parameters of the "sam_kwargs" variable to obtain different results. We recommend accessing the package documentation for a better description of these parameters [Wu and Osco, 2023a]. The feature mask, with a spatial resolution of 2x2 meters, generated for the entire region of interest, was subsequently used to obtain channels, edges, roads and boundaries within and between the fields applying to classified irrigated rice areas (see **Figure 4**). Although the original mask contains various features for all the geometries found in the image, we chose to use only the irrigated rice areas based on our Sentinel-2 binary map generated in Section 2.6 as a delimiter to extract roads, irrigation channels, and boundaries, since our interest is in monitoring these irrigated rice areas.

2.5 Evaluation metrics

The qualitative analysis of the five generated blocks was carried out by inspecting how well the generated maps included the channels, borders, and roads that are located between and within the irrigated rice fields. This inspection was carried out by comparing the generated maps with an RGB reference image and the created reference map. Furthermore, a macro-level qualitative analysis was performed to assess the overall presence of false-positive and false-negative area inclusions. This was particularly focused on regions where irrigated rice cultivation is not feasible, such as built-up areas and forests.

The generated binary map was assessed not only by overall accuracy, but also recall, precision, and the F1 score derived from the confusion matrix. Accuracy serves as a fundamental metric in classification assessment; however, relying solely on accuracy can be insufficient for a comprehensive evaluation. Therefore, in addition to accuracy, precision, recall and the F1 score are used as essential evaluation criteria [Zhang *et al*., 2019].

The general accuracy gauges the relationship between the model predictions and the total instances across all test sets, calculated as the equation (1).

$$\text{Accuracy} = \frac{\text{TP} + \text{TN}}{\text{TP} + \text{TN} + \text{FP} + \text{FN}} \tag{1}$$

Precision represents the ratio of truly positive instances among all predicted positive cases, calculated as equation (2).

$$\text{Precision} = \frac{\text{TP}}{\text{TP} + \text{FP}} \tag{2}$$

In contrast, recall signifies the proportion of all actual positive instances correctly predicted as positive, determined by Equation (3). In particular, precision and recall often exhibit a trade-off; an increase in one typically corresponds to a decrease in the other.

$$\text{Recall} = \frac{\text{TP}}{\text{TP} + \text{FN}} \tag{3}$$

The F1 score, a holistic assessment metric that combines precision and recall, is calculated as Equation (4). The F1 score, which is the harmonic mean of precision and recall, offers a balanced perspective, with 1 indicating optimal performance and 0 indicating the least desirable outcome.

$$\text{F1 Score} = \frac{2 \times \text{Precision} \times \text{Recall}}{\text{Precision} + \text{Recall}} \tag{4}$$

2.6 Time series extraction and evaluation

To evaluate the time series, the classified areas of irrigated rice for each of the methods described above, as well as the reference areas, were used. The regions of interest (rice fields) were used as a search filter on the Google Earth Engine (GEE) platform from July 1, 2021 to June 30, 2022. Sentinel-2 (COPERNICUS/S2_SR_HARMONIZED) images with cloud filtering and noise-corrected pixels were used. The average values of the Normalized Difference Vegetation Index (NDVI) were extracted for each plot, forming time series for each of the binary maps produced. The extracted series were exported in CSV format for subsequent analysis.

The NDVI index was selected to evaluate the development of rice in the region due to its widespread recognition and established use in agricultural research. Numerous studies have well-documented the behavior of NDVI in rice and other crops monitoring, making it a reliable indicator for this purpose [Amani *et al*., 2020], [ANA, 2020], [Orynbaikyzy *et al*., 2022].

Subsequent analyzes include the analysis of the structure of each series for each irrigated rice area defined by each evaluated mapping method. From the generated graphs, we excluded the series that presented noise that impeded the visualization of rice development and opted to keep only those that presented a mix of the spectral response of NDVI of irrigated rice with other vegetation and those of irrigated rice itself. Then, we verified the total number of generated series (without removing noisy series) and the selected series (with the removal of noisy series).

To obtain the plots and extract the series, the binary maps were vectorized so that each neighboring pixel connected to another of the same class was considered a single polygon. In other words, continuous areas where there is no change in class were treated as single plots for each map. This process ensures that adjacent pixels belonging to the same class are grouped together.

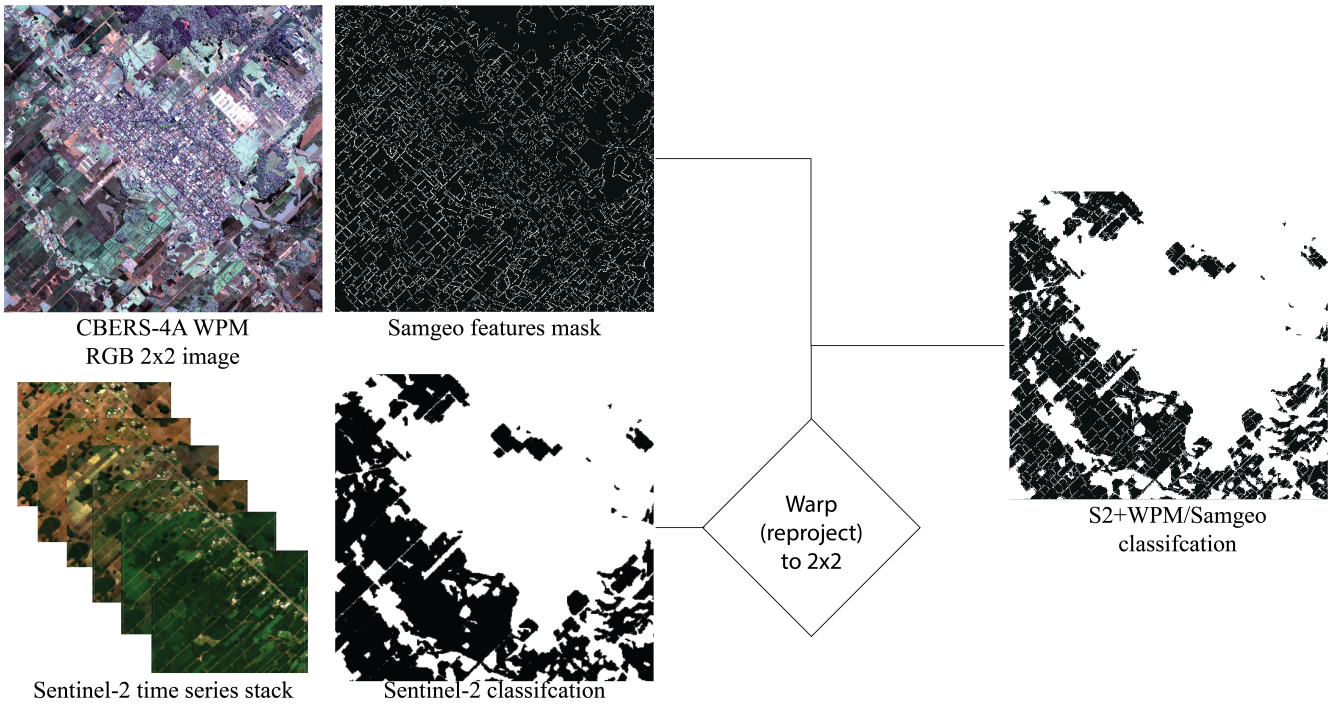

Figure 4. General process to generate an irrigated rice binary map with Sentinel-2/MSI and Samgeo.

3 Results and Discussion

3.1 Qualitative and quantitative analysis

Evaluation of the different classification methods, including Mapbiomas, CBERS4A/WPM, Sentinel-2, and S2+WPM/Samgeo, reveals significant variations in performance compared to a detailed feature map. The Sentinel-2 combined with the WPM/Samgeo method demonstrated superior accuracy (0.879), precision (0.858), recall (0.942), and F1 score (0.895 (**Table 3**), indicating its robust classification capabilities. In contrast, Mapbiomas and CBERS4A/WPM showed lower performance in all metrics, with accuracy scores of 0.767 and 0.752, respectively, and F1 scores of 0.785.

Upon observing the qualitative results (**Figure 5**), it is visually apparent that the binary map derived from the MapBiomas data is capable of identifying the general outline of rice fields; thus, in a macro-analysis, the data appear adequate. However, no channels, boundaries or roads were observed in this classification. This outcome is primarily due to the spatial resolution of the satellite data used of 30 meters.

The results published by [Shimabukuro *et al*., 2023] also recorded that MapBiomas had less accurate results compared to the Land Use Land Cover Random Forest model used by them based on reference polygons created using a Sentinel-2 spatial resolution, highlighting mainly the agriculture class, which showed the highest error of omission, often classified incorrectly as pasture, forest plantation, and forest. This result reinforces the difficulty of differentiating between these classes, which include vegetation targets.

In examining the CBERS/WPM classification, the observations from **Figure 5** reveal that the mapping successfully identified some prominent features, such as wider roads and certain plot boundaries. Compared to MapBiomas mapping, CBERS/WPM offers more detailed delineations within and between rice fields. However, it introduces a notable amount of false positive pixels in the classification, particularly in areas prone to confusion with other crops, grasslands, and fallow lands. The confusion matrix (**Figure 6**) and the (**Table 3**) indicate that the highest commission error was associated with the mapping derived from the CBERS/WPM data, with a precision of 73.2% and an average of 10,719 false positive pixels identified. This was followed by MapBiomas data with a precision of 75.3% and 9,923 false positive pixels on average, Sentinel-2 data with a precision of 78.3% and 9,484 false positives, and S2+WPM/Samgeo with 85.8% precision, representing almost half less false positives at 5,349 pixels on average, i.e. suggests a lower commission error between all models.

This is mainly due to the utilization of a single image for classification and the spectral similarity in vegetation response among these targets. Despite the high comission errors, the channels and roads surrounding and intersecting the irrigated rice fields typically have widths ranging from 2 to 4 meters, making their identification feasible with this product, as can be seen in **Figure 7**. In addition, note that the number of plots is significantly higher compared to the reference areas.

This primary confusion issue that can also be observed in our multiclass map (**Figure 8**) was related to the targets of irrigated rice fields, grasslands, other crops, and fallow land, similar results was highlighted by [Shimabukuro *et al*., 2023] with their Random Forest models for LULC classification. These targets or landscape components were occasionally confused with each other, as observed, for example, within the city image where areas labeled as other crops and irrigated rice were mistakenly classified when they should have been classified as grasslands or trees. Within fallow

lands and other crop areas, some points were also incorrectly classified as irrigated rice, similarly occurring within certain forest regions, where small clusters of pixels were identified as rice.

The main reason for confusion in identifying vegetative areas is due to chlorophyll behavior in green leaves. As [Segarra *et al*., 2020] noted, chlorophyll strongly absorbs blue and red light in the visible spectrum (400–700 nm) for photosynthesis. Meanwhile, leaves reflect and transmit more in the near-infrared (700–1300 nm) due to their structure and biomass. Additionally, the plant canopy structure and leaf surface area crucially affect reflectance patterns, important for monitoring growth

Although the incorporation of more detailed features into our CBERS/WPM classification is beneficial in that it effectively delineates these features compared to MapBiomas, the these false positives makes our classification less suitable: the irrigated rice area within the study area suffers from significant overestimation errors. Moreover, while MapBiomas lacks finer-scale features like roads, channels, and the boundaries of rice plots, and; hence, further suitable than CBERS/WPM as it contains a fewer number of false positive inclusions.

In terms of classification accuracy (**Table 3**), our results indicate that Sentinel-2 exhibits a lower false positive rate in the class of irrigated rice compared to CBERS/WPM, but a higher rate compared to MapBiomas. Notably, the incorporation of temporal series data significantly reduces the incidence of false positive inclusions, even when using lower resolutions such as 30x30 pixels in the case of MapBiomas and 10x10 pixels in our Sentinel-2 model. In contrast, the use of a single CBERS/WPM image results in a higher rate of false positives. These findings highlight the potential benefits of integrating temporal series data into satellite imaging applications for improved accuracy and reduced errors.

A classification based on a single image is particularly desirable in regions with high cloud cover and noise. In this regard, achieving high-accuracy classification with a CBERS-4A image would be ideal, given the cloud coverage in our study area. However, the random forest model applied here failed to provide an accurate classification. One potential solution for the region could be the use of hyperspectral images, which allow area characterization by extracting hundreds of spectral features from a single image, as demonstrated in the case of wheat and rapeseed by [Meng *et al*., 2021]. Furthermore, the incorporation of other techniques or algorithms such as semantic segmentation models based on clusters or deep-learning methods may enable the use of a single image or a combination of unique images from different sources for agricultural mapping, as reported by [Luo *et al*., 2023].

Although the Sentinel-2 and MapBiomas models, in a macro analysis, successfully classify and differentiate rice fields from other targets, they cannot identify detailed features of irrigation channels, roads and plot boundaries, which are more prevalent when employing our approach that combines Sentinel-2 binary classification with the feature mask generated by Samgeo.

As [Cucho-Padin *et al*., 2020] highlight in their research, accurate mapping is crucial for small-scale farmers, who produce around 70% of the world's food. Unfortunately, national crop statistics often do not accurately capture the diverse cropping systems used by small farmers. This lack of precision makes it difficult for policymakers and farmers to make informed decisions about food production and distribution. A system that collects accurate crop data from the farm level would revolutionize crop management and prevent food shortages. Although satellite technology is used for monitoring, its spatial resolution is often too coarse to capture the diverse crops grown by small-scale farmers. To support these farmers and ensure global food security, it is crucial to improve mapping accuracy using advanced remote sensing. This would enable better monitoring, more efficient resource allocation, and a more secure food supply.

Table 3. Performance of each classification compared to detailed features map.

Metric	Mapbiomas	CBERS4A	Sentinel-2	Sent2+Samgeo
Accuracy	0.767	0.752	0.814	0.879
Precision	0.753	0.732	0.783	0.858
Recall	0.837	0.868	0.943	0.942
F1	0.785	0.785	0.853	0.895

Our Sentinel-2 model also suffers from vegetation confusion, and to better understand this the **Figure 9** exhibits the temporal behavior for each band used in the model. Areas identified as fallow and other crops exhibit similar spectral behavior from July to December. During the first two months, the NIR reflectance in these areas is around 0.2. By mid-October, it peaks at 0.4 before dropping to approximately 0.2 for fallow areas and 0.3 for other crop areas. In fallow areas, this peak is due to the spontaneous growth of herbaceous and natural plants, and the subsequent drop occurs due to their removal and soil preparation for new crops. This pattern is evident in the red (B4) and shortwave infrared (B11 and B12) bands, where reflectance values increase after mid-April, indicating exposed dry soil following vegetation removal.

In contrast, for areas with other crops, after the mid-October vegetative peak and subsequent drop in reflectance, the red and SWIR bands stabilize. This indicates an increase in absorption in these bands due to the presence of vegetative and reproductive parts of the plant and water from irrigation. In the short-wave infrared region (SWIR) from approximately 1300 to 2500 nm, radiation absorption is mainly influenced by the water content and other biochemical components of leaves, as observed by [Segarra *et al*., 2020] and [Holzman *et al*., 2021]. In agriculture, factors such as seasonal climatic changes, extreme weather events, pests, soil properties, and phenological stages alter plant signal patterns. For irrigated rice, the SWIR band is particularly sensitive to water levels at the beginning and early stages of the season.

From the images, it is evident that the number of lines and features representing non-rice classes is significantly higher in the S2+WPM/Samgeo image compared to other evaluated methods.

Among the primary limitations of our proposed method is its reliance on the Sentinel-2 classification to delineate irrigated rice fields, leading to cases where only the mask is applied over channels and roads, leaving parts of the edges unmasked. This creates polygons that show a mixture of rice with other materials present at the edges, such as asphalt,

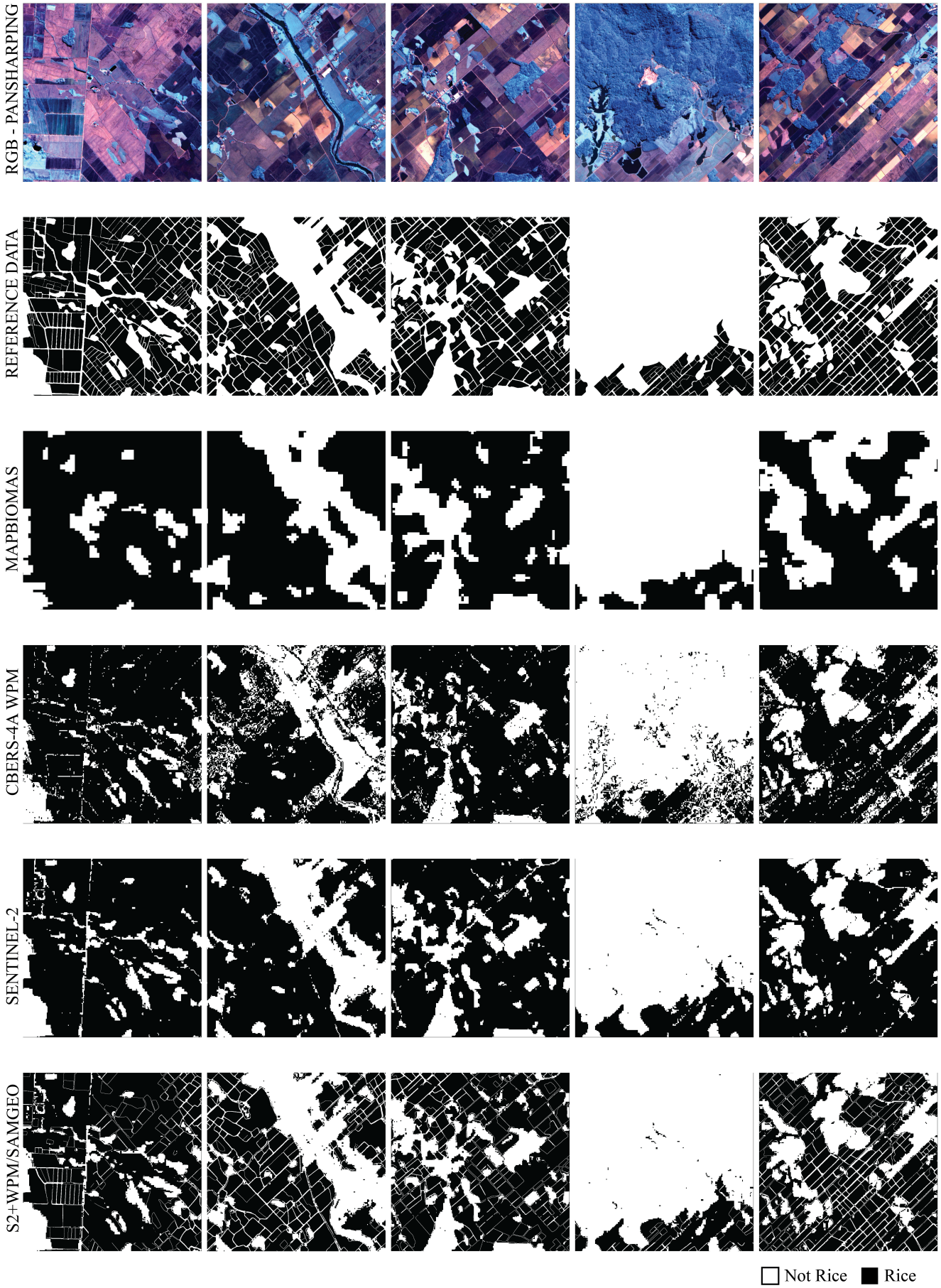

Figure 5. Qualitative results of binary irrigated rice classification by different approaches.

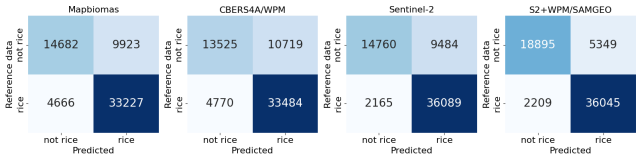

Figure 6. Confusion matrix for the different evaluated irrigated rice fields maps based on 62,500 pixels.

exposed soil, and other types of vegetation, as can be seen in **Figure 7**. Additionally, the Samgeo zero-shot segmentation model fails to distinguish some internal plots, especially when pixels demonstrate homogeneity among neighborhoods, resulting in excessively extensive geometries that require manual adjustment.

To address these issues in future endeavors, it is recommended, if possible, to utilize a minimum of two CBERS images, one for the initial period and another for the final stage of rice development. This ensures that neighboring pixels are at different stages, enabling the creation of more heterogeneous plots, which should enhance the mask obtained by Samgeo. Another alternative is to employ higher-resolution images, such as Planet images, to obtain more detailed information on each irrigated rice area.

The effect of borders in crop fields is a well-known phenomenon, as demonstrated by previous studies, such as those conducted by [Gomez and De Datta, 1971] and [Vernertti *et al*., 1982], which highlight the importance of identifying field borders and selecting rice cultivars that are better adapted to border conditions, which typically receive less fertilizer and exhibit lower productivity.

More recent work by [Wang *et al*., 2013] investigated the effects of field borders on rice grain yields and found that the overestimation rate decreased with larger plot sizes. They concluded that the rate of overestimation of the minimum yield due to the border effect was 2.7%. This finding is consistent with other research by [Castro Álvarez *et al*., 2013] and [Zheng *et al*., 2023], which reported yield overestimation ranging from 3% to 20% as a result of effects of the border and the plot sizes.

In agricultural remote sensing studies, recognizing the importance of borders and based on the agronomic insights discussed above, it is not uncommon. In some studies, researchers apply a negative buffer to exclude field borders from their analyses, regardless of the type of crop [Reyes *et al*., 2023], [Beriaux *et al*., 2021], [Orynbaikyzy *et al*., 2022]. The purpose of applying this exclusion buffer is to avoid the inclusion of heterogeneous pixels in the time series analysis, which can result from the incorporation of adjacent materials such as exposed soil, irrigation dikes, and different types of vegetation [Reyes *et al*., 2023], or even due to the different management practices employed by farmers at the field borders [Beriaux *et al*., 2021]. This practice ensures more accurate and consistent data for remote sensing analyzes, enhancing the reliability of the results.

In terms of our Sentinel-2 model, the top 14 variables produced the most accurate rice irrigation map for the 2021/2022 season (**Figure 10**). The training step achieved an accuracy of 99.25%, indicating a high level of accuracy in correctly predicting both classes. In the validation step, the model demonstrated an accuracy of 94.4%, further confirming its performance. The analysis of the F score enabled the verification that among the 24 variables used, the bands B11_stdDev (SWIR) and B8_mean (NIR) showed an importance above 5% in classification (**Figure 10**). These two bands are of great importance due to the characteristics in which the landscape/image is found during the early stages of development (up to a vegetative peak) of irrigated rice cultivation. Regarding B11_stdDev, since the fields are irrigated by flooding, the SWIR1 values undergo significant changes during the transition from completely flooded fields at the beginning of planting to completely dry fields at the end of harvesting. Therefore, when computing the standard deviation of the values of each pixel in the image, there is a significant difference between the values obtained in the first image of the temporal series and the last image. Regarding B8_mean, it is of great importance to differentiate rice fields from other areas, since rice exhibits variation in the mean due to variations in green pigmentation (high interaction with the NIR band), while other targets such as forests, exposed soil, water and urban areas have a more constant value for this band.

It should be noted that among the first 14 bands, which represent the cumulative importance of 63% for classification, three are related to band B11 (SWIR) (stdDev, min and mean), three are related to band B8 (NIR) (stdDev, min, and mean), two are related to band B4 (Red) (stdDev and min), two are related to band B12 (SWIR2) (stdDev and min), two are related to band B2 (Blue) (stdDev and max), and two are related to band B3 (Green) (stdDev and mean). The images generated from the extraction of maximum values in the temporal series showed the lowest overall importance, with only band B3_max among the top 14 bands of importance. On the other hand, images generated from the extraction of standard deviation values from the temporal series were of the highest importance. So, for all bands, the stdDev is among the top 14 most important parameters.

Their importance can be attributed to the dynamic nature of plant growth, which undergoes substantial changes from exposed soil to the vegetative peak stages [Boschetti *et al*., 2017]. This fluctuation in the reflectance values of the pixels results in higher standard deviation values within the rice areas. Furthermore, complete removal of vegetation during soil preparation and sowing phase facilitates the distinction between crop fields and other surfaces, as evident in **Figure 9**. Consequently, the minimum pixel values in the time series become crucial in classifying rice areas, as they capture the distinctiveness of these stages in the vegetation cycle.

From the reduction of the variables used in the model, the classification image was generated that returns the highest validation accuracy with 14 variables (94.4%). The use of three and four variables only resulted in a classification with 1.2% and 1.3% lower accuracy, while the classification with only the two most important variables returned a classification with 3.8% lower accuracy. Between 5 and 23 variables, the difference in the best accuracy (14 variables) did not exceed 0.74%. Therefore, it is interesting to note that the use of all variables (24) returned a classification 0.9% less accurate. Some studies indicate that the correct selection of variables and the number of variables for the RF model is ideal for producing good results [Bazzan *et al*., 2022; Badda *et al*., 2023]. Contrary to intuition, increasing the number of variables for

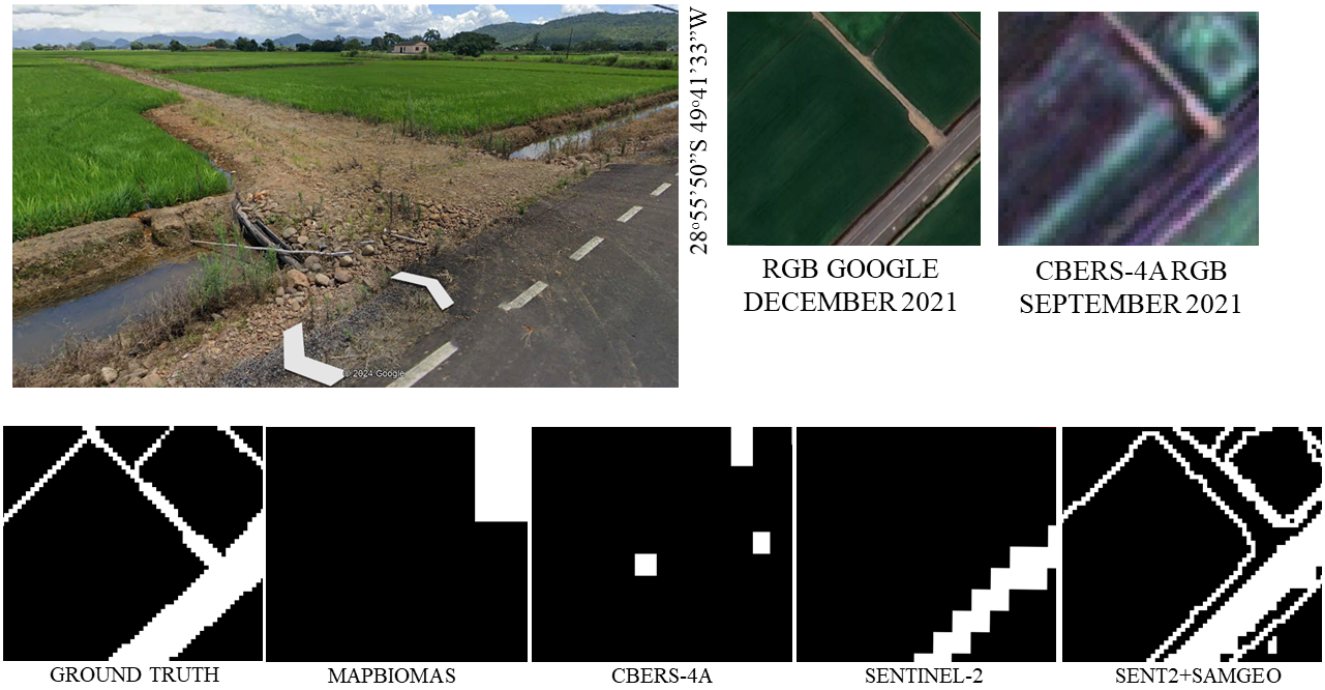

Figure 7. Example of how the detailed features in the irrigated rice fields looks like in different maps.

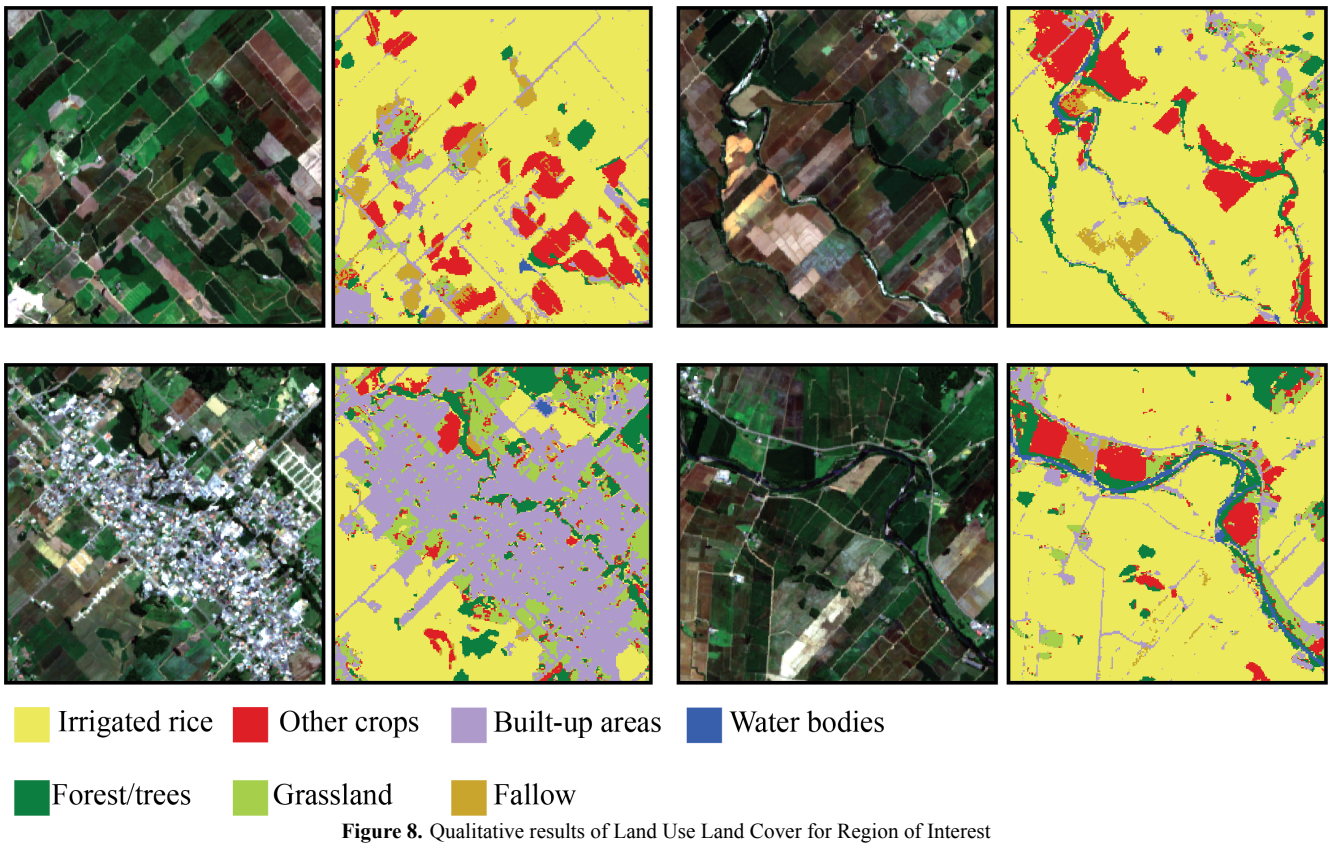

Figure 8. Qualitative results of Land Use Land Cover for Region of Interest

the model can reduce its accuracy.

We understand that our S2+WPM/Samgeo model, which combines a binary map generated by our model to classify Sentinel-2 data with a single CBERS-4A/WPM image, is crucial to improve the final results of the S2+WPM/Samgeo map. Therefore, the analyses conducted in this study contribute to the development of a better model for future work.

3.2 Time series analysis

To classify and identify rice growing areas, it is acceptable to use a map with a broader delineation of plots since the main

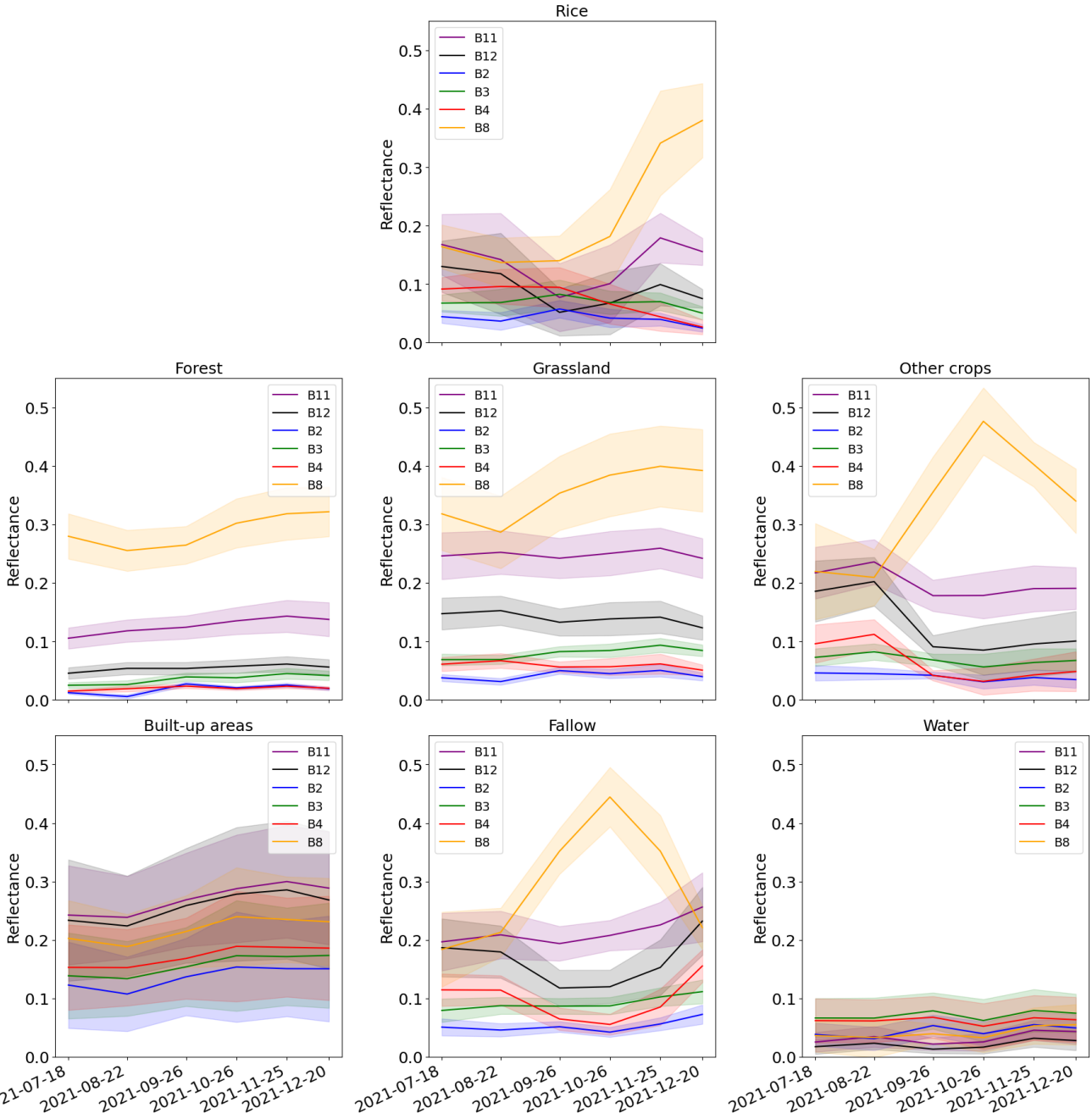

Figure 9. Spectral response of each Sentinel-2/MSI bands for different Land Use Land Cover classes in the Region of Interest

objective is to locate rice producing regions and differentiate them from other objects in the scene/image. However, by encompassing a large area in the classification, we can include different patterns (time series behavior) of irrigated rice cultivation, for example, short cycle and long cycle rice, early and late-sowed irrigated rice, or even single-cycle or regrowth-cycle rice (double harvest), as discussed next.

In the temporal series analysis, the number of plots and, consequently, the NDVI patterns of irrigated rice development obtained from each mapping source varies considerably (**Figure 11**). The reference map initially presented a total of 1334 rice plots; however, after the removal of series that displayed extreme cloud or shadow noise, which hindered pattern identification, the observed series dropped to 1325.

For the MapBiomas binary map, the original number of plots was 26, and after the removal of noisy series, the count decreased to 25. Regarding series originating from the CBERS4A/WPM map, the initial count was 626, but numerous noisy series were observed, reducing the count to 260, representing the highest number of removed series compared to the original count.

Sentinel-2 mapping yielded a total of 99 NDVI temporal series, with only 48 identified as noise-free for irrigated rice. The Sent2+Samgeo binary map generated the highest number of NDVI series and plots for irrigated rice compared to the reference data, with an initial count of 982 patterns, reduced to 847 after the removal of noisy series.

In **Figure 11**, the main observed behaviors are represented through the grouping of noise-free plots from the utilized mappings. Upon analyzing the patterns obtained, it is ev-

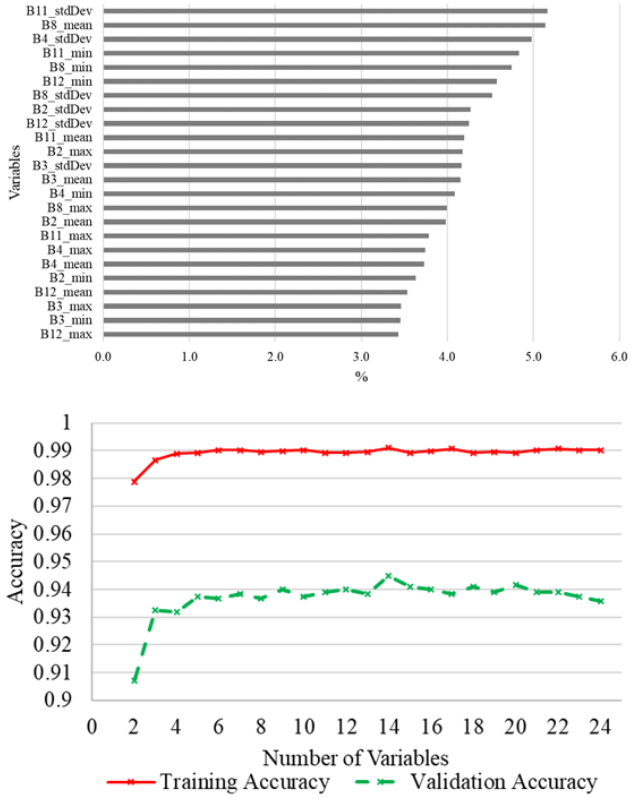

Figure 10. Analysis of the importance (%) of the variables used in the Random Forest (upper) Sentinel-2/MSI classification. Evaluation of training and validation accuracy as a function of the reduction in the number of variables inserted into the model (bottom).

ident that the reference map reveals four distinct patterns, two primarily distinguished by a single rice crop cultivation and the other two showing regrowth, indicating two harvests within the same season. Focusing solely on these behaviors (single or double cropping), the distinguishing factors among them are the curve's amplitude, flattening, and temporal shift (early, regular, or late onset of cultivation). These differences in curves are mainly due to the use of different cultivars, varying fertilization strategies, and agricultural management practices by farmers.

The region is characterized by the implementation of multiple rice cultivars. A study conducted by [Macarini *et al*., 2019] in the Southern region, near the municipalities of Morro Grande, Turvo, and Meleiro, revealed that 55% of farmers use the SCS121 CL cultivar (long cycle), followed by the SCS122 MIURA cultivar (long cycle) at 24%, and the SCS116 SATORU cultivar (medium cycle) with 10%, with the remaining four cultivars collectively accounting for 12% of the total planted area in the region.

In general, the time series data obtained from the rice plots in the MapBiomas project accurately represent the development patterns of the crops in the region. However, we observe a double harvest pattern in which the NDVI signal is much more prominent in the second peak compared to the first. This suggests a mix of different types of vegetation within a single plot classified as irrigated rice, as rice regrowth does not exhibit such a marked increase as observed in the reference plot curves.

A similar pattern is evident in one of the behaviors derived from the binary map of Sentinel-2 data, which also shows two distinct peaks. Furthermore, some behaviors in Sentinel-2 data exhibit an almost linear NDVI pattern, indicating noise within the plots classified as irrigated rice. These more linear NDVI patterns suggest the presence of perennial vegetation, which only shows variation due to seasonal changes, unlike irrigated rice.

The patterns obtained from the CBERS plots show the noisiest data, with many linear behaviors included. Despite the mixed vegetative targets in the CBERS binary map plots, it is still possible to observe growth and decline at the beginning and end of the series. This highlights the difficulty of the model used to differentiate irrigated rice from grasslands, other crops, and fallow.

Compared to the reference NDVI series, the temporal patterns obtained from the Sent2+Samgeo mapping are the most similar and thus quite satisfactory. In these patterns, we can observe both single and double cultivation, although the series are slightly flatter.

Studies involving NDVI time series for smallholders generally use unmanned aerial vehicles (UAVs) to monitor individualized agricultural areas. This mapping generally allows the acquisition of images for only a few properties, assessing variations within individual plots [Stoy *et al*., 2022] and evaluating the costs of flights with the benefits of monitoring [Harsh *et al*., 2021]. The approach we propose can aid in the monitoring of small irrigated rice plots, even at the city or state level, as it incorporates techniques that allow the individual separation of rice fields.

At the regional level and on larger scales, the study conducted by [Guan *et al*., 2016], which monitored irrigated rice in Vietnam, showed that there can be up to four variations of cultivation in the region. In contrast, the work of [Csillik *et al*., 2019], which monitored various crops in two regions in California and Texas, highlighted the significant regional variability and indicated that understanding small-scale temporal series can facilitate crop mapping. Furthermore, the study by [Bellón *et al*., 2017] showed that knowledge of the temporal series of a vegetation index like NDVI on a regional scale can enable the differentiation of rice from other crops in a region of Tocantins, Brazil.

To illustrate how classification using larger rice plots can affect the observation of detailed time series behaviors, we use the example of an area depicted in **Figure 12**. Three different cultivation patterns are presented in **Figure 12**, found within a single plot defined as rice area by Sentinel-2 approach (without the application of the Samgeo segmenter). On the other hand, it can be observed that the larger plot shows an overall average behavior for the entire covered region, with NDVI values equivalent to 0.1 on 2021/08/22, 0.7 on 2022/02/18, and 0.3 on 2022.

The three plots selected to represent the heterogeneity found within a single plot classified with broad delineation are identified with IDs 37, 38, and 101. Plots 37 and 101 exhibit behavior similar to the overall average for 2021/02/22, with an NDVI value of 0.1. However, plot 38 shows a slightly lower value close to 0; this difference can also be seen in **Figure 12** (left image), where plots 37 and 101 reflect a darker and browner coloration, indicating a wetter and waterlogged soil, characteristic of recently irrigated soils. However, plot 38 for the same date shows a more yellowish and

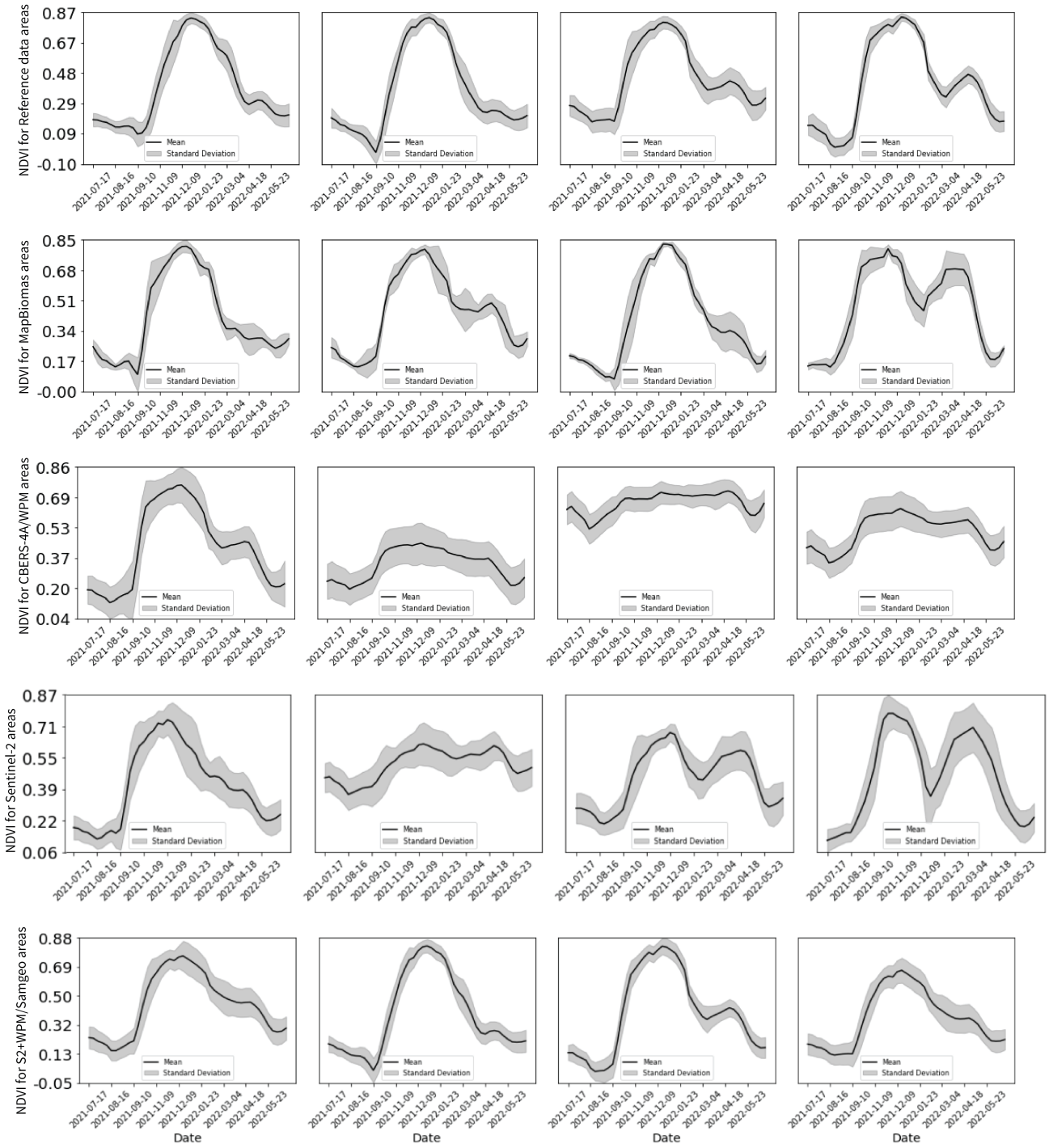

Figure 11. Comparison of most observed behaviors of Sentinel-2/MSI NDVI time series using different binary of irrigated rice maps.

light coloration, characteristic of exposed and dry soil.

On the date of 2021/02/18, plots 37 and 101 also exhibit more similar behavior with elevated NDVI values (0.8 and 0.75, respectively), indicating the presence of rice plants with high vegetative vigor and high reflectance in the NIR band, meaning the plants are still in the field and have not yet been harvested, as seen in the image and their respective time series. However, plot 38 shows a sharp decrease for 2021/02/18 with an NDVI close to 0.3, indicating the removal of plants from the field, i.e. harvesting.

Analysis of the time series and images in **Figure 12** reveals a double harvest behavior in plot 38 due to the increase in the NDVI value between March and May, with green coloration present in the image on 2021/05/19. Plots 37 and 101 exhibit a single-cut difference pattern with harvest around April. The main difference between these two plots is that plot 37 shows a crop development pattern starting in early October, while the development in plot 101 already begins in mid-September. In this sense, in the image of 2021/05/19, it is possible to observe more exposed soil in plot 101, while in plot 37 a darker/greener coloration is noticed, indicating the presence of crop residues.

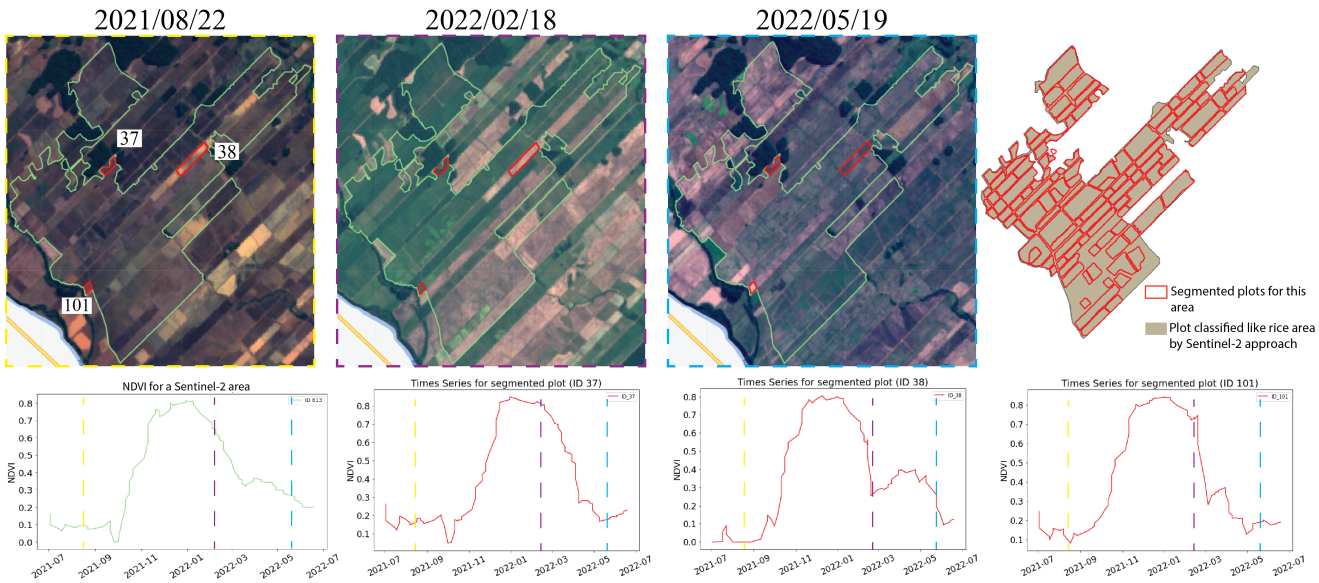

Figure 12. Temporal profile of individually segmented plots compared to a large plot obtained through Sentinel-2 classification.

A more specific investigation with a more local analysis of the plots allows for better estimation of planting and harvesting dates with precision. Furthermore, possible planting failures due to natural phenomena and attacks by pests or pathogens can also be better evaluated with a more detailed segmentation of the plots, compared to a broad or average classification of the plots. As discussed earlier, more effective segmentation is obtained by using higher-resolution images. Therefore, since medium-resolution images, such as Sentinel-2, are more frequent (6-day revisit time), allowing for better crop monitoring, they are suitable for producing maps with broad plots. Complementarily, CBERS-4A images (less frequent revisits) can optimize the segmentation of classifications produced based on 10x10 m/px Sentinel-2 images, as demonstrated in this study.

Typically, the identification of small features in the agricultural field employs techniques utilizing images from UAVs [Padua *et al*., 2024], [Brinkhoff *et al*., 2018], and [Traore *et al*., 2022]. However, employing a technique such as generating a mask through high-resolution imagery, like that of CBERS-4A/WPM, to map these features - such as irrigation channels, roads and boundaries - allows for expanded coverage of these mappings. This approach improves the ability to monitor and manage agricultural landscapes in larger areas, utilizing the high spatial resolution of CBERS imagery to accurately capture and delineate critical infrastructure and plot divisions within the agricultural context.

In addition to enabling individual monitoring of irrigated rice fields through better delineation, the identification of irrigation channels offers some other benefits. Facilitates improved regional planning to reduce or prevent damage caused by leaks [Padua *et al*., 2024] and [Traore *et al*., 2022]. Furthermore, it allows the appropriate management of invasive aquatic plant species that clog and infest channels [Brinkhoff *et al*., 2018]. This precise mapping and monitoring capability is essential to maintain efficient water distribution and ensure the sustainability of agricultural practices.

4 Conclusion

In conclusion, our evaluation of classification methods has shown that Sentinel-2 combined with Samgeo approach stands out as the most effective, achieving an accuracy of 87.9%, precision of 85.8%, recall of 94.2%, and F1 score of 89.5%. In contrast, Mapbiomas and CBERS4A demonstrated lower accuracy scores of 76.7% and 75.2%, respectively, with corresponding F1 scores of 78.5%. Mapbiomas struggled to identify detailed features due to its coarse spatial resolution, while CBERS4A introduced a significant number of false positives, particularly in areas confused with other vegetation types. Furthermore, our analysis of time series data revealed notable variations in the number of plots identified, with the Sent2+Samgeo method generating the highest count of 847 noise-free patterns, indicating its efficacy in capturing temporal dynamics. These results highlight the importance of integrating high-resolution temporal data and advanced segmentation techniques for accurate agricultural mapping, which is crucial to supporting small-scale farmers.

Acknowledgements

This study was financed in part by the Coordenação de Aperfeiçoamento de Pessoal de Nível Superior - Brasil (CAPES) - Finance Code 001. This study was also supported by Conselho Nacional de Desenvolvimento Científico e Tecnológico (CNPq) (PhD scholarship to A.D.B.G, and grant PQ-310042/2021-6 to I.D.S) and São Paulo Research Foundation (FAPESP) (grant 2021/07382-2 to M.E.D.C.).

Authors' Contributions

AG and VP are the main contributors and writers of this manuscript. IS contributed to the writing, conceptualization, and review. MC contributed to the conception and writing of this study. DT contributed to the methodology and review. KT contributed to the analysis, review and reference data of the study. All authors read and approved the final manuscript.

Competing interests

The authors declare that there isn't a conflict of interest.

Availability of data and materials

The datasets and scripts of the current study are available at https://github.com/Dalla01/Segmentation_SamGeo_RiceFields

References

Amani, M., Kakooei, M., Moghimi, A., Ghorbanian, A., Ranjgar, B., Mahdavi, S., Davidson, A., Fisette, T., Rollin, P., Brisco, B., and Mohammadzadeh, A. (2020). Application of Google Earth Engine Cloud Computing Platform, Sentinel Imagery, and Neural Networks for Crop Mapping in Canada. *Remote Sensing*, 12(21):2072–4292. DOI: https://doi.org/10.3390/rs122135611.

ANA (2020). Mapeamento do arroz irrigado no Brasil. Technical report, Agência Nacional de Águas e Saneamento - ANA.

Badda, H., Cherif, E. K., Boulaassal, H., Wahbi, M., Alaoui, O. Y., Maatouk, M., Bernardino, A., Coren, F., and El Kharki, O. (2023). Improving the Accuracy of Random Forest Classifier for Identifying Burned Areas in the Tangier-Tetouan-Al Hoceima Region Using Google Earth Engine. *Remote Sensing*, 15(17):4226. DOI: https://doi.org/10.3390/rs15174226.

Bazzan, T., Rennó, C, D., Lima, D. L. C., and Reckziegel, E. W. (2022). Integração da incerteza na amostragem e classificação Random Forest utilizando bandas e índices espectrais para o mapeamento de inundação. *Geociências*, 41(4):905–925. DOI: https://doi.org/10.5016/geociencias.v41i04.16802.

Bellón, B., Bégué, A., Lo Seen, D., De Almeida, C. A., and Simões, M. (2017). A remote sensing approach for regional-scale mapping of agricultural land-use systems based on ndvi time series. *Remote Sensing*, 9(6):600. DOI: https://doi.org/10.3390/rs9060600.

Beriaux, E., Jago, A., Lucau-Danila, C., Planchon, V., and Defourny, P. (2021). Sentinel-1 time series for crop identification in the framework of the future cap monitoring. *Remote Sensing*, 13(14):2785. DOI: https://doi.org/10.3390/rs13142785.

Boschetti, M., Busetto, L., Manfron, G., Laborte, A., Asilo, S., Pazhanivelan, S., and Nelson, A. (2017). PhenoRice: A method for automatic extraction of spatio-temporal information on rice crops using satellite data time series. *Remote sensing of environment*, 194:347–365. DOI: https://doi.org/10.1016/j.rse.2017.03.029.

Brinkhoff, J., Hornbuckle, J., and Barton, J. L. (2018). Assessment of aquatic weed in irrigation channels using uav and satellite imagery. *Water*, 10(11):1497. DOI: https://doi.org/10.3390/w10111497.

Castro Álvarez, R., Morejón Rivera, R., Díaz Solís, S. H., and Álvarez, G. E. (2013). Efecto de borde y la validez de los muestreos en el cultivo del arroz. *Cultivos Tropicales*, 34(2):70–75. DOI: https://tinyurl.com/3yzdz6az.

Clauss, K., Ottinger, M., and Künzer, C. (2018). Mapping rice areas with sentinel-1 time series and superpixel segmentation. *International journal of remote sensing*, 39(5):1399–1420. DOI: https://doi.org/10.1080/01431161.2017.1404162.

CONAB (2023). Acompanhamento da safra brasileira de grãos - Safra 2022/23. Technical Report 9, Companhia Nacional de Abastecimento.

Crisóstomo de Castro Filho, H., Abílio de Carvalho Júnior, O., Ferreira de Carvalho, O. L., Pozzobon de Bem, P., dos Santos de Moura, R., Olino de Albuquerque, A., Rosa Silva, C., Guimaraes Ferreira, P. H., Fontes Guimarães, R., and Trancoso Gomes, R. A. (2020). Rice crop detection using lstm, bi-lstm, and machine learning models from sentinel-1 time series. *Remote Sensing*, 12(16):2655. DOI: https://doi.org/10.3390/rs12162655.

Csillik, O., Belgiu, M., Asner, G. P., and Kelly, M. (2019). Object-based time-constrained dynamic time warping classification of crops using sentinel-2. *Remote sensing*, 11(10):1257. DOI: https://doi.org/10.3390/rs11101257.

Cucho-Padin, G., Loayza, H., Palacios, S., Balcazar, M., Carbajal, M., and Quiroz, R. (2020). Development of low-cost remote sensing tools and methods for supporting smallholder agriculture. *Applied Geomatics*, 12:247–263. DOI: https://doi.org/10.1007/s12518-019-00292-5.

de Bem, P. P., de Carvalho Júnior, O. A., de Carvalho, O. L. F., Gomes, R. A. T., Guimarães, R. F., and Pimentel, C. M. M. (2021). Irrigated rice crop identification in southern brazil using convolutional neural networks and sentinel-1 time series. *Remote Sensing Applications: Society and Environment*, 24:100627. DOI: https://doi.org/10.1016/j.rsase.2021.100627.

FAO (2022). FAOSTAT: FAO Statistical Databases. Available: https://www.fao.org/faostat/en/#data/QCL/visualize. Accessed on: 2022-06-19.

Garcia, A. D. B., Chaves, M. E. D., Prudente, V. H. R., and Sanches, I. D. (2023). Assessing The Influence Of Borders And Roads On The Segmentation Of Rice Fields: A Case Study. In *XXIV Brazilian Symposium on Geoinformatics - GEOINFO 2023, São José dos Campos, SP, Brazil, December 4-6, 2023*, pages 1–12. MCTI/INPE. DOI: https://dblp.org/db/conf/geoinfo/geoinfo2023.html.

Garcia-Pedrero, A., Lillo-Saavedra, M., Rodriguez-Esparragon, D., and Gonzalo-Martin, C. (2019). Deep learning for automatic outlining agricultural parcels: Exploiting the land parcel identification system. *IEEE access*, 7:158223–158236. DOI: https://doi.org/10.1109/ACCESS.2019.2950371.

GDAL and OGR (2024). GDAL/OGR: Geospatial Data Abstraction software Library. Available: https://gdal.org/drivers/raster/vrt.html#gdal-vrttut-pansharpen. Access: 01 may 2024.

Gomez, K. A. and De Datta, S. K. (1971). Border effects in rice experimental plots I. unplanted borders. *Experimental Agriculture*, 7(1):87–92. DOI: https://doi.org/10.1017/S0014479700004816.

Google (2024). Google earth engine developers: Resampling and reducing resolution. Website. Available: https://developers.google.com/earth-

engine/guides/resample. Access: 01 may 2024.

Gorelick, N., Hancher, M., Dixon, M., Ilyushchenko, S., Thau, D., and Moore, R. (2017). Google Earth Engine: Planetary-scale geospatial analysis for everyone. *Remote Sensing of Environment*, 202:18–27. DOI: https://doi.org/10.1016/j.rse.2017.06.031.

Guan, X., Huang, C., Liu, G., Meng, X., and Liu, Q. (2016). Mapping rice cropping systems in vietnam using an ndvi-based time-series similarity measurement based on dtw distance. *Remote Sensing*, 8(1):19. DOI: https://doi.org/10.3390/rs8010019.

Harsh, S., Singh, D., and Pathak, S. (2021). Efficient and cost-effective drone–ndvi system for precision farming. *International Journal of New Practices in Management and Engineering*, 10(04):14–19. DOI: https://doi.org/10.17762/ijnpme.v10i04.126.

Holzman, M. E., Rivas, R. E., and Bayala, M. I. (2021). Relationship between tir and nir-swir as indicator of vegetation water availability. *Remote Sensing*, 13(17):3371. DOI: https://doi.org/10.3390/rs13173371.

Jiang, L., Zhang, B., Ni, Q., Sun, X., and Dong, P. (2019). Prediction of SNP Sequences via Gini Impurity Based Gradient Boosting Method. *Access*, 7:12647–12657. DOI: https://doi.org/10.1109/ACCESS.2019.2893269.

Kirillov, A., Mintun, E., Ravi, N., Mao, H., Rolland, C., Gustafson, L., Xiao, T., Whitehead, S., Berg, A. C., Lo, W.-Y., *et al*. (2023). Segment anything. In *Proceedings of the IEEE/CVF International Conference on Computer Vision*, pages 4015–4026. DOI: https://arxiv.org/abs/2304.02643.

Laborte, A. G., Gutierrez, M. A., Balanza, J. G., Saito, K., Zwart, S. J., Boschetti, M., Murty, M., Villano, L., Aunario, J. K., Reinke, R., *et al*. (2017). Riceatlas, a spatial database of global rice calendars and production. *Scientific data*, 4(1):1–10. DOI: https://doi.org/10.1038/sdata.2017.74.

Li, Q., Wang, C., Zhang, B., and Lu, L. (2015). Object-based crop classification with landsat-modis enhanced time-series data. *Remote Sensing*, 7(12):16091–16107. DOI: https://doi.org/10.3390/rs71215820.

Li, Z., Zhang, H. K., Roy, D. P., Yan, L., Huang, H., and Li, J. (2017). Landsat 15-m panchromatic-assisted downscaling (lpad) of the 30-m reflective wavelength bands to sentinel-2 20-m resolution. *Remote Sensing*, 9(7):755. DOI: https://doi.org/10.3390/rs9070755.

Lobell, D. B., Burke, M. B., Tebaldi, C., Mastrandrea, M. D., Falcon, W. P., and Naylor, R. L. (2008). Prioritizing climate change adaptation needs for food security in 2030. *Science*, 319(5863):607–610. DOI: https://doi.org/10.1126/science.1152339.

Luo, Z., Yang, W., Yuan, Y., Gou, R., and Li, X. (2023). Semantic segmentation of agricultural images: A survey. *Information Processing in Agriculture*. DOI: https://doi.org/10.1016/j.inpa.2023.02.001.

Macarini, D. S., Vieira, A. C. P., Zilli, J. C., and Bruch, K. L. (2019). As cultivares plantadas por pequenos produtores: inovação na cadeia orizícola no sul de Santa Catarina. *Revista de Propriedade Intelectual, Direito Contemporâneo e Constituição*, 13(1):200–219. DOI: http://hdl.handle.net/10183/194759.

MapBiomas (2023). Mapbiomas general "handbook": Algorithm theoretical basis document (atbd). Website. Available: https://brasil.mapbiomas.org/en/download-dos-atbds-com-metodo-detalhado/. Access: 03 may 2024.

Masoud, K. M., Persello, C., and Tolpekin, V. A. (2019). Delineation of agricultural field boundaries from sentinel-2 images using a novel super-resolution contour detector based on fully convolutional networks. *Remote sensing*, 12(1):59. DOI: https://doi.org/10.3390/rs12010059.

Meng, S., Wang, X., Hu, X., Luo, C., and Zhong, Y. (2021). Deep learning-based crop mapping in the cloudy season using one-shot hyperspectral satellite imagery. *Computers and Electronics in Agriculture*, 186:106188. DOI: https://doi.org/10.1016/j.compag.2021.106188.

Orynbaikyzy, A., Gessner, U., and Conrad, C. (2022). Spatial transferability of random forest models for crop type classification using sentinel-1 and sentinel-2. *Remote Sensing*, 14(6):1493. DOI: https://doi.org/10.3390/rs14061493.

Osco, L. P., Wu, Q., Lemos, E. L., Gonçalves, W. N., Ramos, A. P. M., Li, J., and Marcato Junior, J. (2023). The segment anything model (sam) for remote sensing applications: From zero to one shot. *International Journal of Applied Earth Observation and Geoinformation*, 124(1):103540. DOI: https://doi.org/10.1016/j.jag.2023.103540.

Oshiro, T. M., Perez, P. S., and Baranauskas, J. A. (2012). How many trees in a random forest? In *Machine Learning and Data Mining in Pattern Recognition: 8th International Conference, MLDM 2012, Berlin, Germany, July 13-20, 2012. Proceedings 8*, pages 154–168. Springer. DOI: https://doi.org/10.1007/978-3-642-31537-4_13.

Padua, L., Marques, P., Dinis, L.-T., Moutinho-Pereira, J., Sousa, J. J., Morais, R., and Peres, E. (2024). Detection of leak areas in vineyard irrigation systems using uav-based data. *Drones*, 8(5):187. DOI: https://doi.org/10.3390/drones8050187.

Prudente, V. H. R., Martins, V. S., Vieira, D. C., e Silva, N. R. d. F., Adami, M., and Sanches, I. D. (2020). Limitations of cloud cover for optical remote sensing of agricultural areas across South America. *Remote Sensing Applications: Society and Environment*, 20:100414. DOI: https://doi.org/10.1016/j.rsase.2020.100414.

Reyes, F., Casa, R., Tolomio, M., Dalponte, M., and Mzid, N. (2023). Soil properties zoning of agricultural fields based on a climate-driven spatial clustering of remote sensing time series data. *European Journal of Agronomy*, 150:126930. DOI: https://doi.org/10.1016/j.eja.2023.126930.

Segarra, J., Buchaillot, M. L., Araus, J. L., and Kefauver, S. C. (2020). Remote sensing for precision agriculture: Sentinel-2 improved features and applications. *Agronomy*, 10(5):641. DOI: https://doi.org/10.3390/agronomy10050641.

Shimabukuro, Y. E., Arai, E., da Silva, G. M., Hoffmann, T. B., Duarte, V., Martini, P. R., Dutra, A. C., Mataveli, G., Cassol, H. L., and Adami, M. (2023). Mapping land

use and land cover classes in são paulo state, southeast of brazil, using landsat-8 oli multispectral data and the derived spectral indices and fraction images. *Forests*, 14(8):1669. DOI: https://doi.org/10.3390/f14081669.

Stoy, P. C., Khan, A. M., Wipf, A., Silverman, N., and Powell, S. L. (2022). The spatial variability of ndvi within a wheat field: Information content and implications for yield and grain protein monitoring. *PloS one*, 17(3):e0265243. DOI: https://doi.org/10.1371/journal.pone.0265243.

Tang, Z., Wang, H., Li, X., Li, X., Cai, W., and Han, C. (2020). An object-based approach for mapping crop coverage using multiscale weighted and machine learning methods. *IEEE Journal of Selected Topics in Applied Earth Observations and Remote Sensing*, 13:1700–1713. DOI: https://doi.org/10.1109/JSTARS.2020.2983439.

Traore, S., Fipps, G., Swanson, C., Dufek, J., and Robin, M. (2022). Unmanned aerial vehicle system integrating high-resolution sensors for detecting leaks in irrigation canals—proof of concept. *Irrigation and Drainage*, 71(1):206–217. DOI: https://doi.org/10.1002/ird.2641.

Vernertti, V. P., Vernetti, F. d. J., and Silveira Junior, P. (1982). Efeito de bordadura lateral e de extremidades de fileiras, sob dois níveis de nitrogênio, em quatro cultivares de arroz na região sudeste do Rio Grande do Sul, Brasil. *Pesquisa Agropecuária Brasileira*, 17(2):185–194. DOI: https://seer.sct.embrapa.br/index.php/pab/article/view/15588.

Waldner, F. and Diakogiannis, F. I. (2020). Deep learning on edge: Extracting field boundaries from satellite images with a convolutional neural network. *Remote sensing of environment*, 245:111741. DOI: https://doi.org/10.1016/j.rse.2020.111741.

Wang, K., Zhou, H., Wang, B., Jian, Z., Wang, F., Huang, J., Nie, L., Cui, K., and Peng, S. (2013). Quantification of border effect on grain yield measurement of hybrid rice. *Field Crops Research*, 141:47–54. DOI: https://doi.org/10.1016/j.fcr.2012.11.012.

Watkins, B. and Van Niekerk, A. (2019). A comparison of object-based image analysis approaches for field boundary delineation using multi-temporal sentinel-2 imagery. *Computers and Electronics in Agriculture*, 158:294–302. DOI: https://doi.org/10.1016/j.compag.2019.02.009.

Wen, C., Lu, M., Bi, Y., Zhang, S., Xue, B., Zhang, M., Zhou, Q., and Wu, W. (2022). An object-based genetic programming approach for cropland field extraction. *Remote Sensing*, 14(5):1275. DOI: https://doi.org/10.3390/rs14051275.

Wrege, M, S., Steinmetz, S., Reisser Junior, C., Rodrigues de Almeida, I., Garrastazu, M. C., Herter, F. G., Caramori, P. H., Matzenauer, R., Radin, B., Braga, H. J., Pandolfo, C., Prestes, S. D., Rocca da Cunha, G., and Maluf, J. R. T. (2012). Atlas climático da região sul do Brasil: estados do Paraná, Santa Catarina e Rio Grande do Sul, institution = Empresa Brasileira de Pesquisa Agropecuária - Embrapa. Technical report, EMBRAPA.

Wu, Q. and Osco, L. (2023a). Segment-geospatial: samgeo module. Available: https://samgeo.gishub.org/samgeo/?h=samgeo. Access: 01 may 2024.

Wu, Q. and Osco, L. P. (2023b). samgeo: A python package for segmenting geospatial data with the segment anything model (sam). *Journal of Open Source Software*, 8(89):5663. DOI: https://doi.org/10.21105/joss.05663.

Xiao, W., Xu, S., and He, T. (2021). Mapping paddy rice with sentinel-1/2 and phenology-, object-based algorithm—a implementation in hangjiahu plain in china using gee platform. *Remote Sensing*, 13(5):990. DOI: https://doi.org/10.3390/rs13050990.

Xue, Y., Zhao, J., and Zhang, M. (2021). A watershed-segmentation-based improved algorithm for extracting cultivated land boundaries. *Remote Sensing*, 13(5):939. DOI: https://doi.org/10.3390/rs13050939.

Zhang, M., Lin, H., Wang, G., Sun, H., and Fu, J. (2018a). Mapping Paddy Rice Using a Convolutional Neural Network (CNN) with Landsat 8 Datasets in the Dongting Lake Area, China. *Remote Sensing*, 10(11):2072–4292. DOI: https://doi.org/10.3390/rs10111840.

Zhang, X., Wang, Y., Zhang, N., Xu, D., and Chen, B. (2019). Research on scene classification method of high-resolution remote sensing images based on rfpnet. *Applied Sciences*, 9(10):2028. DOI: https://doi.org/10.3390/app9102028.

Zhang, X., Wu, B., Ponce-Campos, G. E., Zhang, M., Chang, S., and Tian, F. (2018b). Mapping up-to-date paddy rice extent at 10 m resolution in china through the integration of optical and synthetic aperture radar images. *Remote Sensing*, 10(8):1200. DOI: https://doi.org/10.3390/rs10081200.

Zheng, C., Wang, Y.-c., Xu, W.-b., Yang, D.-s., Yang, G.-d., Yang, C., Huang, J.-l., and Peng, S.-b. (2023). Border effects of the main and ratoon crops in the rice ratooning system. *Journal of Integrative Agriculture*, 22(1):80–91. DOI: https://doi.org/10.1016/j.jia.2022.08.048.